IMPROVE 3D VISUALIZATION FROM RADIOGRAPH FOR C-ARM X-RAY APPRATUS USING SART

Chuchart Pintavirooj* and **Manas Sangworasil**,

ABSTRACT

Cone-beam reconstruction (CBR) is growing in importance, 3D model of the bone, the stack of cross-sectional images can be reconstructed from a series of X-ray radiographs, served as its projections. It has, in certain scenarios, many advantages over the more popular Filtered Backprojection (FBP) approaches and has also recently been shown to perform well for 3D cone-beam reconstruction. In this paper, the Simultaneous Algebraic Reconstruction Technique (SART) is engaged for reconstructing tomograms in case of limited views of radiographs. Compared with well-known FBP algorithm, the SART to acquire the quality of image in the case of limited views, 3D visualization is rendered by the Volume rendering technique with the shading effects.

Keywords: Image Reconstruction; Backprojection; SART; Volume Rendering; Radiograph

1. INTRODUCTION

The image reconstruction is useful for producing volume images from projections in many modalities including SPECT, PET, Multi-slice CT and a C-Arm x-ray apparatus. The clinical applications that show important profit from this technique is 3-D rotational angiography to call cone-beam reconstruction (CBR), applied to the diagnosis and treatment in image-based. Ideally, high-resolution, high-contrast imaging would be obtained and converted into a 3-D image with CBR. Recently, many articles have addressed the computations involved in CBR, including papers by Yu et al.1, Siewerdsen et al.2, Ross et al.3, and Hampton and Hamler4. Although Feldkamp filtered backprojection is the most often discussed algorithm, it has well-known shortcomings; consequently other CBR approaches are often implemented and evaluated5, 6, 7.

Manuscript received on January 29, 2008 ; revised on May 8, 2008.

* Corresponding author.

C. Pintavirooj and M. Sangworasil with Research Center for Communication and Information Technology (ReCCIT), and Department of Electronics, Faculty of Engineering, King Mongkut's Institute of Technology Ladkrabang, Thailand.

E-mail addresses: kpchucha@kmitl.ac.th (C. Pintavirooj) and ksmanas@kmitl.ac.th (M. Sangworasil)

In this paper, we propose the 3D visualization from X-ray radiographs by deriving the stack of cross section from the filtered backprojection technique (FBP) and Algebraic Reconstruction Technique (ART) [9-10]. Sequence stack of cross-section image can be rendered the 3D visualizations, so-called volumetric data, by the rendering technique.

2. SIMULTANEOUS ALGEBRAIC RECONSTRUCTION TECHNIQUE

The Algebraic Reconstruction Technique (ART) is inherently a pixel-based reconstruction algorithm, i.e., a grid correction is based on the projection and backprojection of a single image pixel at a time. This is usually performed via image-order projection methods, i.e., the volume are projected by casting rays into the volume, pixel by pixel. However, salt and pepper noises apparent signify the data caused by ruggedly interpolating of the weighting function. The Simultaneous Iterative Reconstruction Technique (SIRT) can reduce the noise, but to exceeding the time cost. The virtues of ART and SIRT seem to combine in the Simultaneous Algebraic Reconstruction Technique (SART) can convert the data to high quality in a few iterations. We shall now briefly describe the individual steps of the SART algorithm, producing a decomposition that will later be emulated in the graphics pipeline. Recall that SART reconstructs a volume by a series of grid projections and grid corrections. Fig.1 shows a grid voxel contributes to a projection and backprojection, respectively. The volume is decomposed into a field of 3D interpolation kernels through each grid voxel and attenuated by the voxel's value vj. During projection (and backprojection), field is traversed by projection rays ri, connecting the x-ray source with the image pixels pi. The weight factor has on one of these rays is the integral of the traversed voxel kernel function. When projection is pending, rays traverse the voxel kernels and accumulating the weighted voxel contributions into the ray integrals. The ray integrals are subtracting and computed to grid correction factors from the pixel values pi in the sample image P . Then the grid corrections are obtained, that can be thought as smearing all ray across a 2D-plane.

The projection equation of the SART can express mathematically as the following (see Fig. 1.).

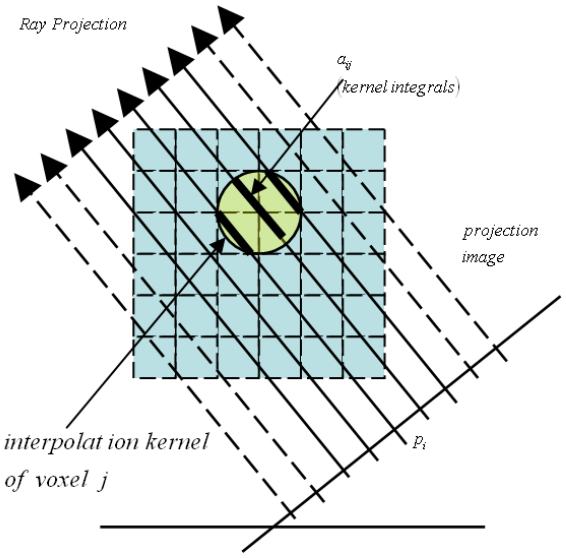

Fig.1: *The interpretation of a voxel weight factor* a_{ij}

$$p_i \approx \sum_{m=1}^{M_i} \hat{f}(s_{im})\Delta s \tag{1}$$

, where p_i is the projection for the i^{th} ray, Δs is the arbitrary equidistance between two lattice's elements, and $f(s_{im})$ is determined from 4 adjacent pixels $(f_j's)$ by bilinear interpolation, or given by

$$\hat{f}(s_{im}) = \sum_{j=1}^{N} d_{ijm} f_j \tag{2}$$

coefficient d_{ijm} remarks the contribution of the j^{th} pixel to the m^{th} point on the i^{th} ray. Substituting Eq. 2. into Eq. 1. yields

$$p_i = \sum_{j=1}^{N} a_{ij} f_i \tag{3}$$

$$a_{ij} = \sum_{m=1}^{M_i} d_{ijm}\Delta s \tag{4}$$

a_{ij} is clearly the weighting function of j^{th} pixel associated with the i^{th} ray. After the projection equation was modeled, the formula for updating the j^{th} pixel on the reconstruction grid for the $(k+1)^{th}$ iteration can be derived as in the case of the ART, the SART is performed for each voxel and grid correction k steps, that written as

$$v_j^{(k)} = v_j^{k-1} + \lambda \frac{\sum_{p_i P_\varphi} \left[\frac{p_i - \sum_{n=1}^{N} w_{in} v_n^{(k-1)}}{\sum_{n=1}^{N} w_{in}} \right] w_{ij}}{\sum_{p_i \epsilon P\varphi} w_{ij}} \tag{5}$$

where the summation with respect to i is for all rays in one projection. The complicated equation can be explained step-by-step as the following:-

(a) Find the weight a_{ij} from Eq. 4. for all pixel j within ith ray.

(b) Calculate the summation of i or numeration term in Eq. 5., the summing is done for rays within one projection. Note that, for the first iteration, the initial values of f_j are normally set to zeros.

(c) Update the f_j's by Eq. 5.

(d) Move to the next projection, repeat (b) and (c). Do this repeatedly until all projections are completed. This is counted as one iteration.

(e) Repeat (b) to (d) by using the same weight as (a) for the succeeding iterations.

3. PROJECTION AND BACKPROJECTION

SART algorithm decomposes the volume into slices and treats each slice separately. In grid projection, each slice is associated with volumetric slice content it. A projection image is obtained by accumulatively each voxel. Here, a bilinear interpolation kernel is used to resample the image into screen coordinates. The ray's integrals so computed are obtained from cone-beam projection equation, the rotated coordinates $(p, s, \zeta)$from (x, y, z) with the axis p and the elevation axis ζ is written as

$$R_\beta(p, \zeta) = \int_{s_m}^{s_m} f(p, s, \zeta) ds \tag{6}$$

$R_\beta(p, \zeta)$ is the shadow-gram of the object that are obtained to projection data by using the radon transform. Views of the projected are angle β and ζ is the elevation axis, the direction of ray's integrals according to axis s.

For the backprojection stage in cone-beam, that is obtained by summing the contribution to the object from all the tilted fan beams equally detectors. The fan is necessary the plane out of the object, the coordinate system of the reconstructed point specify by size of the object show as Fig. 1, that can be changing the parameter by the distance from the center of rotation to source D_{so}. The backprojection equation of cone-beam is now written as

$$f(x, y, z) = \int_0^{2\pi} \frac{D_{so}}{\sqrt{D_{so}^2 - s^2}} R_\beta'(p, \zeta) d\beta \tag{7}$$

$$R'_{\beta}(p,\zeta) = R_{\beta}(p,\zeta)\frac{D_{so}}{\sqrt{D_{so}^2+\zeta^2+p^2}} \tag{8}$$

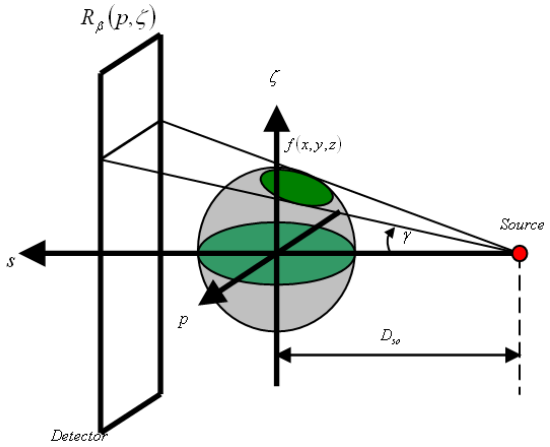

Fig.2:

4. SEEK OF CENTER DETECTOR

The projection data in each view for cone-beam reconstruction method is the two dimension array of detectors that emphasize the center of rotation before reconstructed the object, we will present the method for seek it when the projection data is blundered. In this work the center in the projection data is mistaken by the hardware system that is occurred from the windows capturing on the computer. We will seek the location of center by the shading approximation method.

In Fig.3, (a) is an x-ray radiograph of the box model from a C-Arm x-ray apparatus that is demonstrated the cone-beam by shade of the object in Fig. 3. (b) (Top view). Size of the azimuth object show on a scene that is presented by A_o = 4.5 cm and B_o = 4.5 cm. For A_s and B_s are the size of shade, it is to exceed more than the object's size because it is indicated to the cone-beam. When the center of rotation of point source is placed on the center of the object, both side (Δs_{l1} and Δs_{r1}) of shade will equally. We is written relation as

$$\tan(\psi_1) = \frac{\Delta sl_1}{L_1} \tag{9}$$

$$\tan(\psi_1) = \frac{\Delta sl_2}{L_2} \tag{10}$$

$$\tan(\psi_1) = \frac{\Delta sr_1}{L_1} \tag{11}$$

$$\tan(\psi_1) = \frac{\Delta sr_2}{L_2} \tag{12}$$

$$\frac{\Delta sl_1}{\Delta sl_2} = \frac{L_1}{L_2} \tag{13}$$

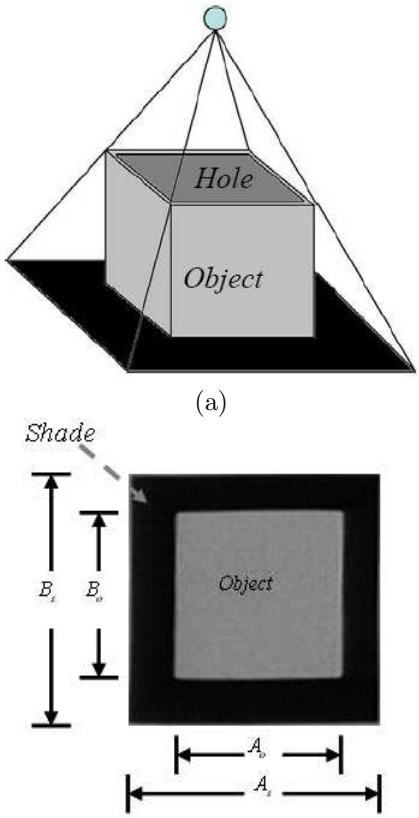

Fig.3:

$$\frac{\Delta sr_1}{\Delta sr_2} = \frac{L_1}{L_2} \tag{14}$$

$$A_o = \Delta sl_2 + \Delta sr_2 \tag{15}$$

$$A_s = \Delta sl_1 + A_o + \Delta sr_1 \tag{16}$$

$\psi_1$and ψ_2 is the inner angles of rays touch the top corner of box show that the relation of length from the point source to scene show in Fig. 4(b). The distance from edges of the box and shade to center rotation are Δs_{l1}, Δs_{l2}, Δs_{r1} and Δs_{r2}. The altitude of box is L_1 and distance from top of box to point source is L_2. Length of box A_o explained by Δs_{l2} and Δs_{r2}, A_o can be obtained from the summation of Δs_{l1}, A_o and sr1. When the point source is shifted that shown in Fig. 4(a), we can be written as

$$\tan(\psi'_1) = \frac{\Delta sl'_1}{L_1} \tag{17}$$

$$\tan(\psi'_1) = \frac{\Delta sl'_2}{L_2} \tag{18}$$

$$\tan(\psi'_2) = \frac{\Delta sr'_1}{L_1} \tag{19}$$

$$\tan(\psi_2^{'}) = \frac{\Delta sr_2^{'}}{L_2} \tag{20}$$

$$\frac{\Delta sl_1^{'}}{\Delta sl_2^{'}} = \frac{L_1}{L_2} \tag{21}$$

$$\frac{\Delta sr_1^{'}}{\Delta sr_2^{'}} = \frac{L_1}{L_2} \tag{22}$$

$$m = \frac{L_1}{L_2} \tag{23}$$

$$A_o = \Delta sl_2^{'} + \Delta sr_2^{'} \tag{24}$$

$$A_s^{'} = \Delta sl_1^{'} + A_o + \Delta sr_1^{'} \tag{25}$$

The stretch of shaded A_s and A_s' are equally distance, we show that by

$$\begin{aligned} A_s &= \Delta sl_1 + A_o + \Delta sr_1 \\ &= m \cdot \Delta sl_2 + m \cdot \Delta sr_2 \\ &= (m+1) \cdot A_o \end{aligned} \tag{26}$$

$$\begin{aligned} A_s^{'} &= \Delta sl_1^{'} + A_o + \Delta sr_1^{'} \\ &= m \cdot \Delta sl_2^{'} + m \cdot \Delta sr_2^{'} \\ &= (m+1) \cdot A_o \end{aligned} \tag{27}$$

In this problem, we need to found sl2' and sr2'when know Ao, As, sl1' sr1' and L1. First, we suppose sl1, sl2, sr1 and sr2, those can be obtained the other parameters such as L1 in (13) or (14) then sl2' and sr2' is obtained by (21) and (22). For this, As = 4.5 cm, Ao = 4.5 cm, Bs = 4.5 cm, Bo = 4.5 cm, sl1' = 1.2375 cm, sr1' = 1.0125 cm and L1 = 30.6 cm, sl2' is 2.475 cm and sr2' is 2.025 cm. The other side we are solved from Bo and Bs which the results are shown center of the point source in Fig. 5.

5. 3D VISULAIZATION IN MEDICAL IMAGING

With the different characteristics, surface rendering and volume rendering [18-19] play an important role in 3D visualization for medical imaging. Surface rendering is used to visualize the shape of the object and the spatial relation among the objects. In this method, the surface of the object are defined and modeled by a number of polygons or other geometric primitives through segmentation or surface detection scheme, followed by the calculation of the normal vector for each polygon. These primitives are then rendered using the computer graphic technique for geometrical object. Volume rendering is quite different; it allows the entire volume to be visualized in the transparent manner. This is achieved by mapping the intensity value to color and alpha channel, to form a colored jelly-like material, which can be rendered by weighting and integrating for each pixel element. Volume rendering provides a better mechanism for displaying weak or fuzzy surfaces and internal structures. On the other hand, it is more computationally expensive than the surface rendering.

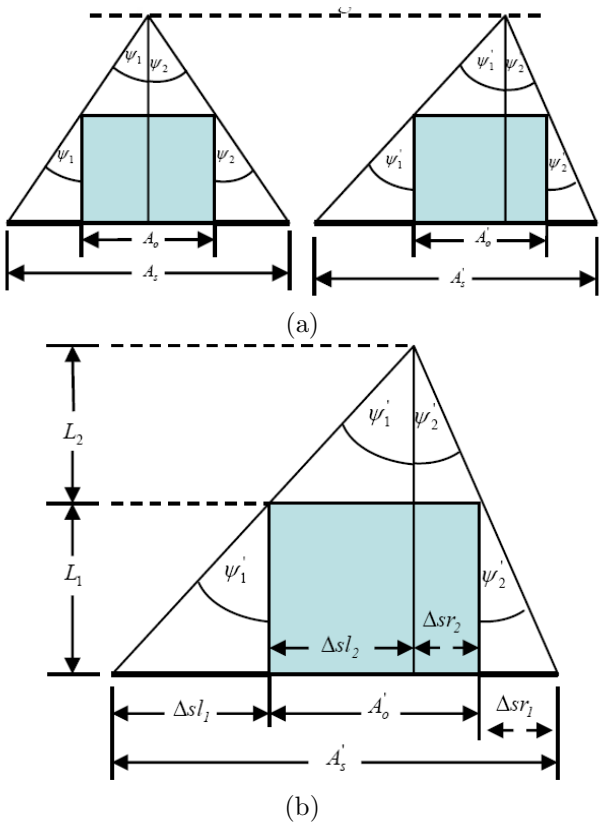

Fig.4:

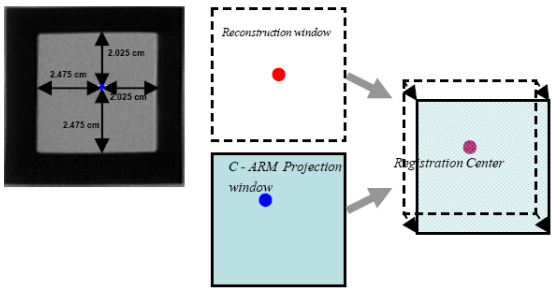

Fig.5:

6. EVALUATION OF FBP AND SART

In order to evaluate the algorithms of FBP and SART, it is suggested to use the Shepp-Logan phantom model as a cross-sectional function. The simulation is setup to reconstruct the phantom from the 12 projections with the 256×256 samples per projection. If size of the phantom function is $256 \times 256 \times 256$ voxels, the number of unknown variable would be 16,777,216.

Hence, the equation is underdetermined by 95.31%. Succession of the algorithm is judged from the time consumption and the mean square error

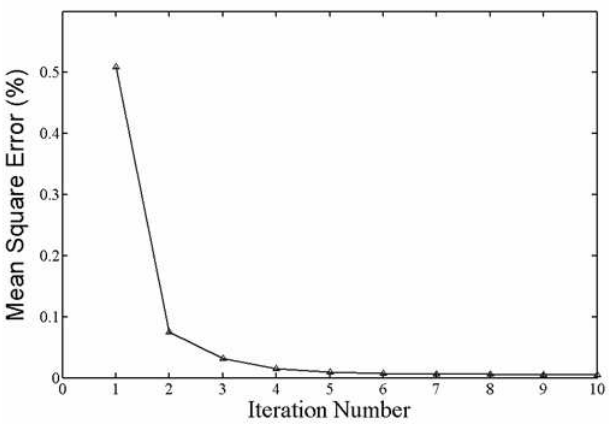

Fig.6: *Iteration number and mean square error of the reconstructed phantom using SART.*

(MSE) of reconstruction, or.

$$MSE = \frac{\int\int \left[o(\vec{r}) - o^{'}(\vec{r})\right]^2 d\vec{r}}{\int\int \left[o(\vec{r})\right]^2 d(\vec{r})} \qquad (28)$$

where $o(r)$ is the actual phantom, and $o'(r)$ is the reconstruction. (The specification of the testing computer is as the following: - Intel Pentium 4 - 2.4GHz, RAM 256 Mbytes, simulation program written by C++ running on Windows platform.)

Time usage for the FBP algorithm in cone-beam method is 83.968 seconds for the entire process with the MSE of the phantom of 7.6585%. The time usage for the SART is 152.32 seconds per iteration, weighting function is calculated in pre-process stage. The plotting of iteration and error is illustrated in Fig. 6. In the first iteration of the SART, an error of phantom is apparently lower than of the FBP algorithm (50.96% compared with 76.585%), and rapidly decays in the few iterations. At the excess of fifth iteration, the error seems stable. Even though the SART takes more time to reconstruct the phantom, its merit of error reduction can be traded off as mentioned before.

Fig. 7 and Fig. 8 display the phantoms at slice number 96 in volume matrix data and theirs corresponding profiles. As one can see in the FBP case, the star artifacts dominate all of the background of phantom; likewise, the DC level is disappeared.

7. 3D RECONSTRUCTION FOR C-ARM X-RAY APPARATUS

From the prior section, SART have been proved to reconstruct the cross section with superiority to the From the prior section, SART have been proved to reconstruct the cross section with superiority to the

To collect the radiographs, we have used BV-29 Phillips C-ARM X-ray apparatus. The apparatus is capable of providing a digital-form radiograph and

(a)Actual phantom slice number 96

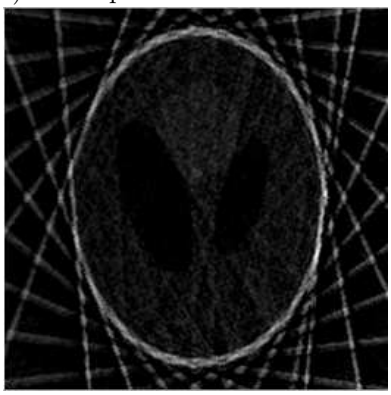

(b)Reconstruction using FBP (83.968 seconds)

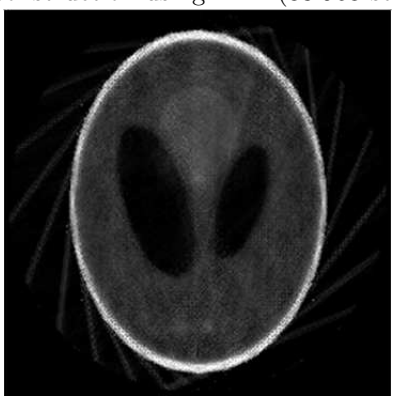

(c)reconstruction using SART with 5 iterations (761.67 seconds)

Fig.7: *The result slice number 96 compared the both algorithms.*

information about the collected angle. The tested phantom is a human femur bone. The number of projection is 36 or 5 degrees per radiograph from 0 to 180 . Figure 9 shows an example of radiographs of femur.

The projected data used for the image reconstruction is extracted from each of the horizontal line of the digitized image. Figure 10 shows sample of reconstructed images using SART. After the reconstruction processes, all of the slices is stacked to form the volumetric data. The volume rendering is then performed on the stacks of data to provide a 3D visualization. After adding the lighting model for more reality, the

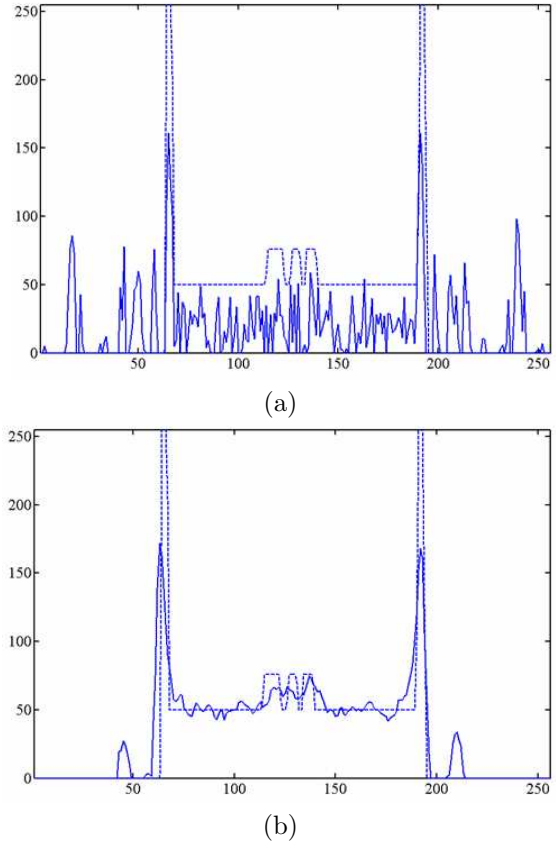

Fig.8: *Profiles from the 208th row and slice number 96 of phantoms (scene of 3 small tumors) by (a) FBP algorithm, (b) SART (dash line is actual phantom, while solid line is reconstruction).)*

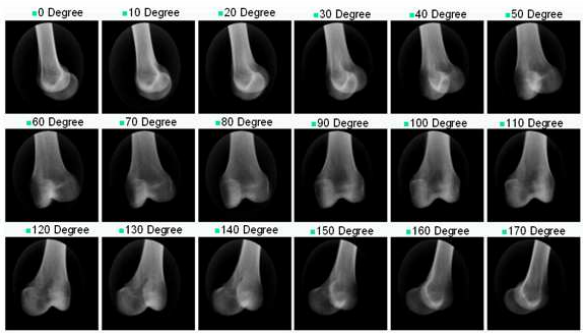

Fig.9: *Sample of X-ray radiographs taken from 60 angles in the half plane.*

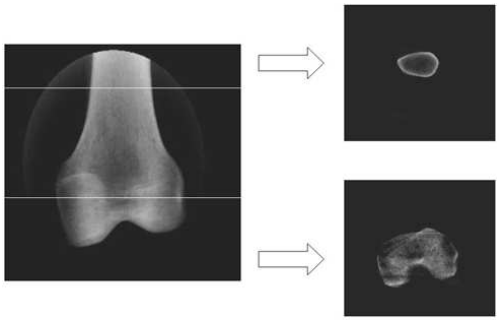

Fig.10: *The cross sections of femur bone reconstructed by the SART.*

3D visualizations are available as shown in Fig. 11.

8. CONCLUSION

The Simultaneous Algebraic Reconstruction Technique (SART) is utilized for reconstructing the cross-sectional image in the case of limited views of projections. At first, this technique is evaluated on the Shepp-Logan phantom with 12 projections. The SART gives the mean square error of 0.5096% in the first iteration within 152.32 seconds, while the FBP gives the error of 7.6585% within 83.968 seconds. The qualities of cross-sectional images from SART algorithm are superior to those from the FBP, with the slightly more time consumption for the SART case.

Note that the SART can further reduce the error in the successive iteration. After the evaluation process, the SART is tested to generate the volumetric data from X-ray radiographs of human femur bone in 36 angles, followed by the volume-rendering technique to display the volume of data in 3D style. The result is very satisfactory.

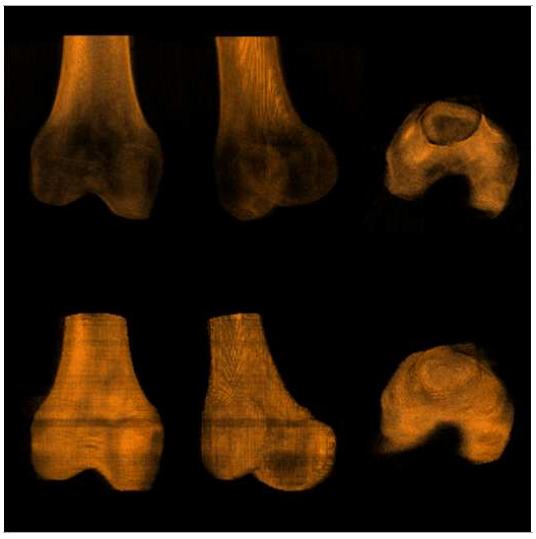

Fig.11: *Three views of the volume rendering of human femur bone using SART.*

9. ACKNOWLEDGEMENT

The researching fund has been kindly supported by the Japan International Cooperation Agency (JICA).

References

[1] D.C. Hemmy, et. al., "Three-dimensional Reconstruction of Craniofacial Deformation using Computed Tomographic," *Neurosurgery*, vol. 13, pp. 534-541, 1983.

[2] W.G. Totty and N.W. Vannier, "Analysis of Complex Masculoskeleton Anatomy using Three-dimensional Surface Reconstruction," *Radiology*, vol. 150, pp. 173-177, 1984.

[3] L. Axel, et. al., "Three-dimensional Display of NMR Cardiovascular Images," *Comput. Assist. Tomography*, vol.7, pp. 172-174, 1983.

[4] N.W. Vannier, et. al., "Three-dimensional Magnetic Resonance Imaging of Congenital Heart Diseases," *Radiographics*, vol. 8, no. 5, pp. 857-871, 1988.

[5] D.N. Levin, et. al., "Integrated Three-dimensional Display of MR and PET Images of the Brain," *Radiology*, vol. 172, pp. 783-789, 1989.

[6] N.J. Valentino, "Volume Rendering of Multimodal Image: Application of MRI and PET image of the Human Brain," *IEEE Trans. Medical Imaging*, vol. 10, no. 4, pp. 554-561, 1991.

[7] R. Pini, et. al., "Echocardiographic Three-dimensional Visualization of the Heart," *NATO ASI Series*, vol. F60, 3D imaging in Medicine, Hohne, K. H. et. al., Eds., Berlin: Springer-Verlag, 1990.

[8] M. Verlande, et. al., "3D Reconstruction of the Beating Left Ventricle and Mitral Valve based on Multiplanar tee," in *Proc. Computers in Cardiology*. New York: IEEE Computer Society Press, 1991.

[9] C. Pintavirooj, C. Ninkaew, M. Sangworasil and K. Hamamoto, "3D Visualization from Radiograph," *ISCIT2001*, pp. 307-310, Nov. 2001.

[10] P. Ungpinitpong, C. Pintavirooj, P. Leartprasert and M. Sangworasil, "Improved 3D Visualization from X-Ray Radiograph Using Algebraic Reconstruction Technique," *ISCIT2002*, Oct. 2002.

[11] A.C. Kak, "Tomographic Imaging with Diffracting and Non-Diffracting Sources," in Array Signal Processing, S. Haykin, Ed. Eaglewood Cliffs, NJ: Prentice-Hall, 1985.

[12] S. Kaczmarz, "Angenaherte Auflosung Von Systemen Linearer Gleichungen," *Bull. Acad. Pol. Sci. Lett. A*, vol. 6-8A, pp. 355-357, 1937.

[13] H. Guan and R. Gordon, "Computed Tomography using Algebraic Reconstruction Techniques (ART) with Different Projection Access Schemes: A Comparison Study Under Practical Situations," *Phys. Med. Biol.*, No.41, pp.1727-1746, 1996.

[14] A.C. Kak and M. Slaney, "Princicles of Computerized Tomographic Imaging," *IEEE Press*, Newyork, 1988.

[15] A.H. Andersen, and A.C. Kak, "Simultaneous Algebraic Reconstruction Technique (SART): A Superior Implementation of the ART Algorithm," *Ultrason. Imaging*, vol. 6, pp. 81-94, Jan. 1984.

[16] R. Gordon, et. al., "Algebraic Reconstruction Techniques (ART) for three dimensional electron microscopy and X-ray photography," *J. Theor. Biol.*, vol. 29, pp. 471-481, 1970.

[17] P. Gilbert, "Iterative Method for the Reconstruction of Three Dimensional Objects from their Projection," *J. Theor. Biol.*, vol. 36, pp. 105-117, 1972.

[18] R.A. Drebin, et. al., "Volume Rendering," *ACM SIGGRAPH Comput.Graph.*, vol. 22, no. 4, pp.65-74, Aug. 1988.

[19] M. Levoy, "Display of Surfaces from Volume Data," *IEEE Comput. Graph. Appl.*, vol. 8, No. 3, pp. 29-37, May, 1988.

C. Pintavirooj was born in Bangkok, Thailand in 1962. He received the B. Sc. (Radiation Techniques) and M.Sc. (Biomedical Instrumentation) from Mahidol University, Bangkok, Thailand in 1985 and 1989 respectively. In 1995, he received another master degree in Biomedical Engineering from Worcester Polytechnic Institute, MA, USA. In 2000, he earned a Ph. D. in Biomedical Engineering from Drexel University, Philadelphia, PA.

After working as a research scientist at Biomedical Instrumentation Department, Mahidol University, he joined Electronic Department, Faculty of Engineering, King Mongkut's Institute of Technology at Ladkrabang, Bangkok where he is currently an associate professor. His current research is in Biomedical Image/ Signal Processing majoring in Image reconstruction, Image Classification and Image restoration.

Dr. Pintavirooj is the acting chairman of Biomedical Engineering Society of Thailand affiliated with IFBME.

M. Sangworasil was born in Bangkok, Thailand in 1951. He received the Bachelor of engineering and Master of Engineering from King Mongkut's Institute of Technology at Ladkrabang, Bangkok, Thailand in 1973 and 1977 respectively, and the D. Eng (Electronics) from Tokai University, Japan, in 1990.

Following his graduate studies, he worked almost 28 years at Electronic Department, Faculty of Engineering, King Mongkut's Institute of Technology at Ladkrabang, Bangkok where he is currently an associate professor. His research interest are in the area of image process with emphasis on Image Reconstruction, 3D modeling, Image Classification and Image Filtering.

Dr. Sangworasil is now the director of Computer and Research Center, King Mongkut's Institute of Technology at Ladkrabang.